Fermi National Accelerator Laboratory

FERMILAB-Conf-91/24-E
[E-740]

DØ Calorimeter Electronics Performance*

The DØ Collaboration

presented by

Marcel Demarteau
State University of New York at Stony Brook
Stony Brook, New York 11794

December 14, 1990

* Presented at the International Conference on Calorimetry in High Energy Physics, Fermilab, Batavia, Illinois, October 29 - November 1, 1990.

Operated by Universities Research Association Inc. under contract with the United States Department of Energy

DØ Calorimeter Electronics Performance

Marcel Demarteau
State University of New York at Stony Brook
Stony Brook, NY 11794

The DØ collaboration

Abstract

A brief description of the DØ Calorimeter Electronics is given and its performance in recent studies at Fermilab described. Measurements of electronic, uranium, and coherent noise made on approximately 10% of the full DØ system are presented. The stability, linearity and dependence on detector capacitance of the amplifier gains are discussed, along with techniques for transferring a test beam calibration of the detector to DØ using the DØ pulser system.

1 Introduction

The DØ experiment exposed three types of endcap calorimeter modules to a calibration beam at Fermilab between May and August, 1990. One of the primary goals of this run was to establish the absolute energy calibration of the calorimeter modules to better than 1% and to transfer that calibration to the full DØ experiment. A crucial aspect in establishing the absolute calibration of the DØ calorimeter is the understanding of the performance of the calorimeter electronics.

During this calibration run sections of the Electromagnetic and Inner Hadronic (IH) module and a Middle Hadronic (MH) module of the DØ endcap calorimeter were tested. The layout of these modules in the test beam together with a discussion of their performance, has been given elsewhere in these proceedings [1, 2] and will not be addressed here. This paper will concentrate on the performance of the DØ calorimeter electronics during this calibration run. Approximately 4000 readout channels were instrumented of which about 1450 channels were in the electromagnetic calorimeter, 2400 in the inner hadronic module and 120 in the middle hadronic module. This constitutes about 10% of the total number of channels of the full DØ calorimeter system.

2 Electronics

The DØ calorimeters consist of absorber plates separated by two, $2.3mm$ thick, liquid argon gaps. Centered in the liquid argon between the absorber plates are signal boards, consisting of copper charge collecting pads sandwiched between $0.5mm$ thick layers of fiber glass epoxy. The outer surfaces of the fiber glass epoxy are coated with a resistive layer. A drift field between the absorber plates, which are at ground potential, and the signal boards is established by maintaining a high voltage of $2.5kV$ on the resistive layers of the signal boards. The embedded copper pads provide a $\Delta\eta \times \Delta\varphi = 0.1 \times 0.1$ segmentation in pseudorapidity and azimuth. Longitudinally, the signals from different cells are ganged, radially in the central barrel calorimeter and along z in the two endcap calorimeters, to form layers of semi-projective towers. These towers contain 4 layers in the EM module and 5 layers in each of the IH and MH modules of the endcap. In the third layer of the electromagnetic calorimeter, approximately at shower maximum, each tower is further subdivided 2×2 times, to provide a $\Delta\eta \times \Delta\varphi = 0.05 \times 0.05$ segmentation.

Signals exit the cryostat through feedthrough ports. Inside the cryostat the signals are ordered according to how the detector was constructed, with many η, φ towers from a particular depth on a single multiconductor cable. The signals are reordered in the feedthrough ports so that all the readout cells of a $\Delta\eta \times \Delta\varphi = 0.2 \times 0.2$ semi-projective tower exit on two adjacent multiconductor cables, facilitating the formation of a fast trigger. Short runs of cables connect the external side of the feedthrough to low noise hybrid charge-sensitive amplifiers (preamps). Two versions of preamps are used, one with a $5pF$ and one with a $10pF$ feedback capacitor. The $10pF$ version is used in layers 3 and 4 of the electromagnetic section of the calorimeter, where the largest signals occur.

The output voltages of the preamps are fed into a shaping and sampling circuit, known as the base line subtractor (BLS) [3]. The shaping in the front end of the BLS hybrid consists of a $430ns$ integration and a $33\mu s$ differentiation. In addition there is a gain of 3 to change full scale from 3.3 Volts at the preamp output to 10 Volts at the sampling stage. With the shaping done, the signals peak between 2 and $2.4\mu s$, depending on the detector capacitance and are relatively flat at $2.2\mu s$. A dual sampling of the signal for baseline subtraction follows the shaping. In test beam operation two analogue memory cells follow the signal until a trigger from scintillation counters upstream in the beam is received. On arrival of the trigger, one memory cell samples the baseline before the suitably delayed calorimeter signal has had a chance to rise, and $2.2\mu s$ later the second memory cell holds the signal. These are the baseline and peak sampling, respectively. The difference signal is sent to the ADC.

Fifteen bit dynamic range is obtained with low cost 12 bit successive approximation ADC's by using precision $\times 8$–$\times 1$ amplifiers, whose gains can be forced into either of the two values, or selected automatically according to the signal am-

plitude. If the difference signal reaching these amplifiers is less than 1.25 Volts it is amplified eightfold and the result digitized by the 12 bit ADC circuitry. Larger signals are digitized directly, with no additional analogue gain, and the resulting ADC output digitally shifted 3 bits [3].

The ADCs digitize 24 input signals simultaneously in about $10\mu s$ and repeat this cycle 16 times to complete digitizing all 16×24 channels in one ADC card. Because of the ×8–×1 amplification the dynamic range of the measurements is 2^{15}. The ADCs reside in a VME crate that reads the outputs into a VME buffer which drives the data cable. The data cable carries the data to the dual-port memories of a set of four micro VAX-II computers.

The ADCs can perform pedestal subtraction and zero-suppression for each channel separately. Although pedestals were downloaded into the ADCs, neither pedestal subtraction nor zero-suppression was done in the ADCs during the test beam run. During the whole running period, pedestal and pulser runs were taken on a regular basis.

3 Noise

The performance of a system with a very large number of electronic channels can be severely affected by sources of noise. Let x_i^α be the ADC output of channel α ($\alpha = 1, \ldots, \mathcal{N}$), for the i-th event ($i = 1, \ldots, \mathrm{N}$). The fluctuations in the signals can then be quantitatively described by forming the sum

$$\begin{aligned} S^2 &= \frac{1}{\mathrm{N}} \sum_{i=1}^{\mathrm{N}} \left(\sum_{\alpha=1}^{\mathcal{N}} (x_i^\alpha - \bar{x}^\alpha) \right)^2 \\ &= \frac{1}{\mathrm{N}} \sum_{i=1}^{\mathrm{N}} \sum_{\alpha=1}^{\mathcal{N}} (x_i^\alpha - \bar{x}^\alpha)^2 + \frac{1}{\mathrm{N}} \sum_{i=1}^{\mathrm{N}} \sum_{\substack{\alpha,\beta \\ \alpha \neq \beta}}^{\mathcal{N}} (x_i^\alpha - \bar{x}^\alpha)(x_i^\beta - \bar{x}^\beta) \qquad (1) \\ &= \sum_{\alpha=1}^{\mathcal{N}} S_{\alpha\alpha} + \sum_{\substack{\alpha,\beta \\ \alpha \neq \beta}}^{\mathcal{N}} S_{\alpha\beta} \end{aligned}$$

Here $\bar{x}^\alpha$ is the mean value of x for events in channel α. The diagonal elements are simply the variances of the signals. The off-diagonal elements indicate if the fluctuations in the signals of channel α are in phase with those of channel β and are a measure of the coherent noise. Assuming for simplicity that every channel has the same random noise σ^2 and that the cross-correlation between every pair of channels (α, β) is equal to c^2, the sum in equation 1 can be written as

$$S^2 = \mathcal{N}\sigma^2 + \mathcal{N}(\mathcal{N}-1)c^2$$

The coherent noise term, $\mathcal{N}(\mathcal{N}-1)c^2$, grows quadratically with the number of channels and becomes equal to the random noise when $\mathcal{N} = \sigma^2/c^2$ signals are added.

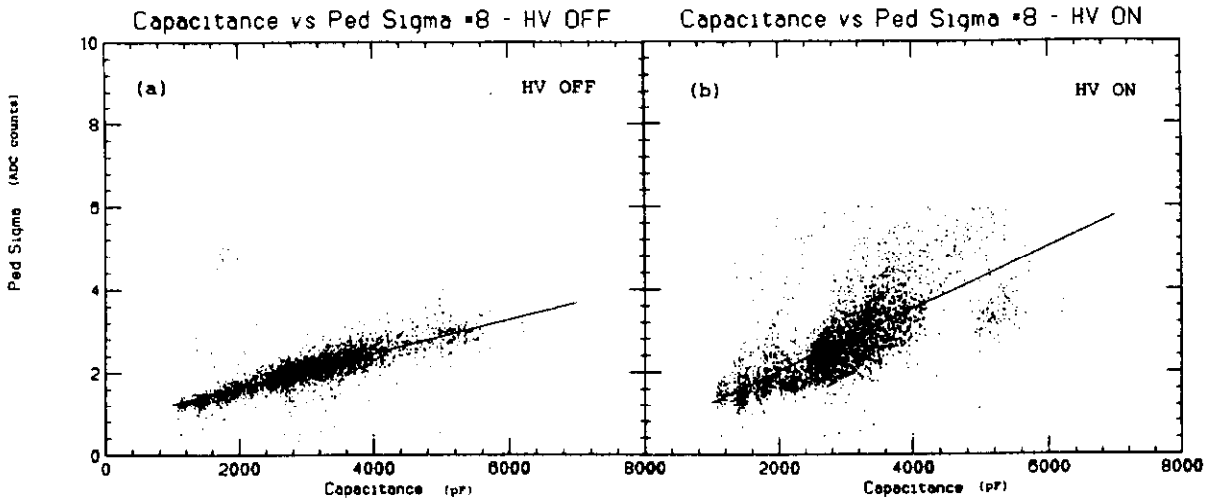

Figure 1: Widths of pedestals taken in $\times 8$-mode versus detector capacitance for the case the high voltage on the signal boards is turned off (a), and the high voltage is turned on (b).

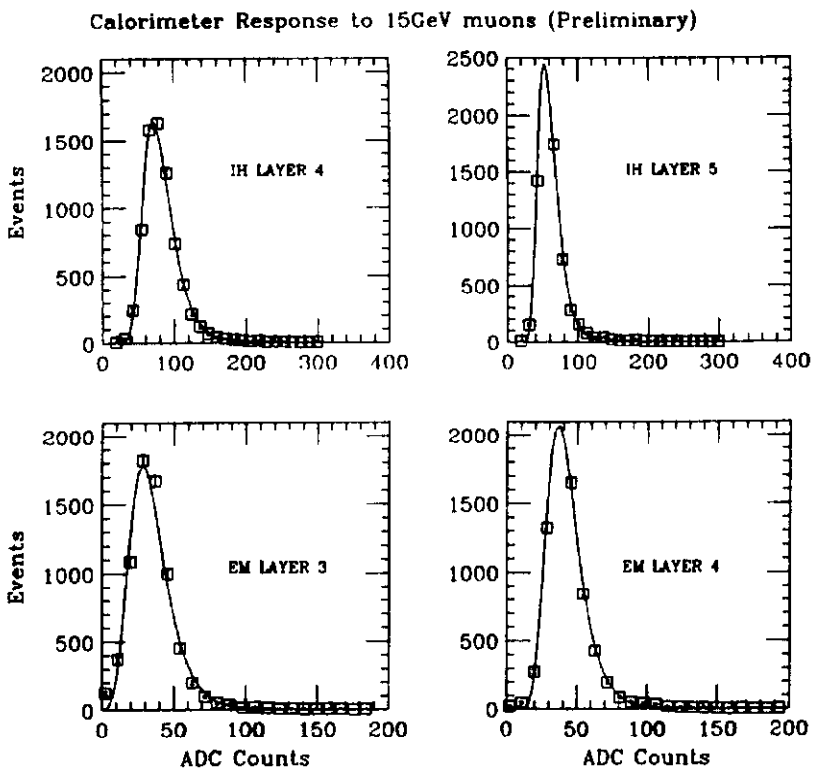

Figure 2: Distributions of energy deposited by $15GeV$ muons in layers 4 and 5 of the IH module and in layers 3 and 4 of the EM module.

The rms noise voltage measured by the ADC is proportional to the noise density and the bandwidth of the system, and is linear in the total readout cell capacitance [4]. Figure 1a shows the distribution of the sigma of the pedestals, taken in $\times 8$-mode, versus the detector capacitance C_D for the case the high voltage on the signal boards is turned off. The linear dependency on the detector capacitance can be seen clearly. The random noise per channel corresponds to about 150-200μV at the preamp output. It should be noted that $100\mu V$ correspond to approximately one ADC count, which represents a charge of 3000 electrons at the preamp input. Figure 1b shows the same scatter plot with the high voltage applied to the signal boards. The broader scatter, which is apparent in this case, is due to the Uranium noise. It is interesting to note that for some channels the pedestal width is the same for both cases. These channels, which are the channels with a large cell capacitance, are the readout channels of the coarse sections of the calorimeter modules that use stainless steel as absorber.

It has been possible to keep the coherent noise in this setup low to the level of 5-7μV per channel. This corresponds to a negligibly small charge of about 150 electrons per channel at the preamp input. The number of channels that can be added before the coherent noise starts to dominate is 600 - 1600 channels. As an illustration of the very low noise levels in the system, figure 2 shows the response of four different depth segments of the calorimeter to $15GeV$ muons. As is clear, minimum ionizing particles can be detected unambiguously in the calorimeter. Normalizing these distributions to the amount of liquid argon seen by the muon for each layer in the calorimeter, the signal of a minimum ionizing particle is about 12 ADC counts per centimeter of liquid argon.

4 Pulser Performance

4.1 Introduction

Connected to the input of each preamp channel is a precision resistor which allows measuring the relative response of all channels with a pulser (see figure 3) [5]. The main components of the pulser system are a current source, an attenuator box, which controls the amplitude of the injected charge, and a coaxial switch box. During a pulser calibration run the system steps through the 32 switch positions of the switch box, with 144 channels connected to each position of the switch. A set of 144 channels is in the following referred to as a pulser pattern.

Given an input voltage $V(t)$ at the pulser input to the preamp, the output voltage is given approximately by

$$V_{out} = \frac{\int V(t)\,dt}{RC_F} \quad \frac{AC_F}{AC_F + C_D} \tag{2}$$

where C_F is the feedback capacitance, C_D the detector capacitance, R the feedback resistance and A is the DC open loop gain of the preamp. To ensure an equal

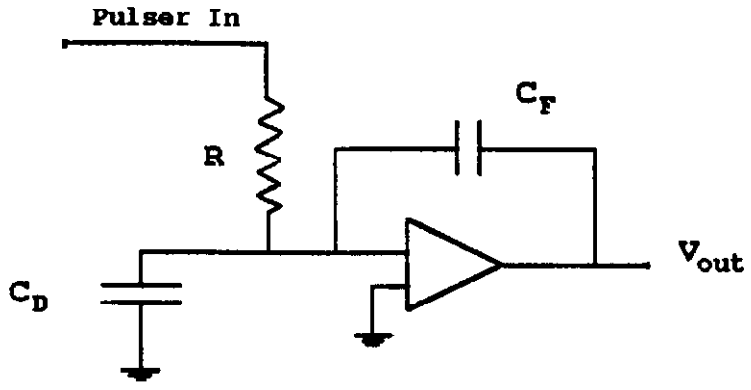

Figure 3: Schematic of the pulser input to the DØ calorimeter preamp.

response of all channels the values for the resistances have been chosen to be $499k\Omega$ and $249k\Omega$ for the $5pF$ and $10pF$ channels, respectively. The capacitance of the readout cells ranges from 1.5 to $5.0nF$ and the DC open loop gain of the preamp is about 3500. The width of the pulse from the pulser is about $300ns$.

4.2 Linearity

Pulser runs at a series of attenuator settings have been taken to study the linearity of the gains. Since the difference signal between the peak and baseline sampling is processed through $\times 8$–$\times 1$ amplifiers, two sets of gain values are obtained. For every channel the output ADC value, corrected for the detector and feedback capacitance according to equation 2, has been fitted to a straight line for both the $\times 1$ and $\times 8$ amplification region separately. The results for a randomly chosen channel are shown in figure 4a. Plotted here is the ADC output versus pulser amplitude. Though the pulser amplitude is in arbitrary units, the pulser covers an energy range from 2.5 to $50GeV$. Figure 4b shows the deviations from a straight line fit for all channels for the $\times 1$ amplification region. The deviations from linearity for all channels are less than $\pm 0.25\%$. The channel-to-channel relative response for a given pulser amplitude has an rms spread of $\approx 2.3\%$.

4.3 Stability

During the running period the temperatures of the BLS and preamp systems were being read out and recorded at the beginning of each run. The temperature that was read out was a time average over the preceding 10 minutes. The temperature data consists of 60 BLS temperatures, 10 temperature sensors for each of the 6 BLS crates, and 6 preamp temperatures. The temperature variations of the cooling water had a 5 minute cycle time. Because of the short cycle time, the temperature changes at the BLS and preamp were pretty well averaged out. It is estimated that the residual temperature fluctuations at the electrical components is of the order of 0.25°C.

To study the gain stability events from a single pulser pattern of 144 channels were used. Figure 5a shows the time dependence of the gain of a particular channel normalized to the average gain for the 144 channels in this pulser pattern.

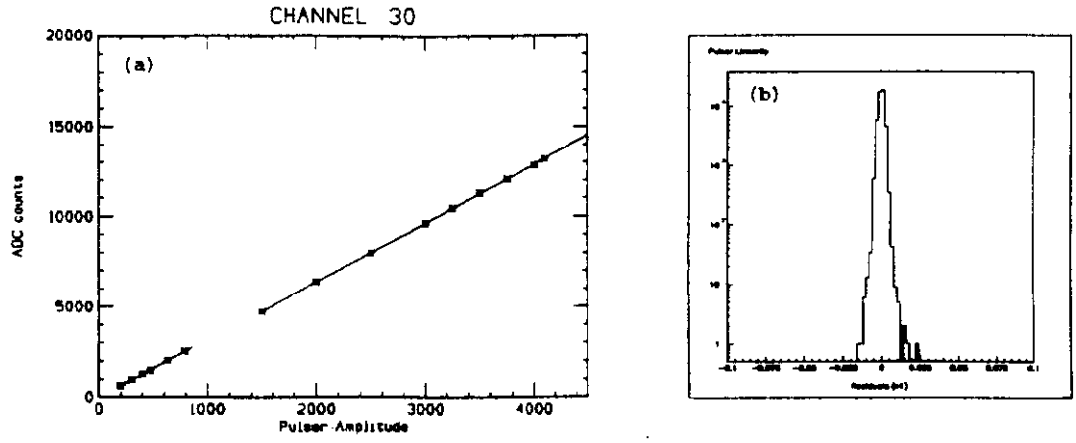

Figure 4: (a) Response of a single channel to different pulser amplitude settings. The pulser amplitude is in arbitrary units. (b) Deviations from linearity of the gains taken in $\times 1$-mode for all channels.

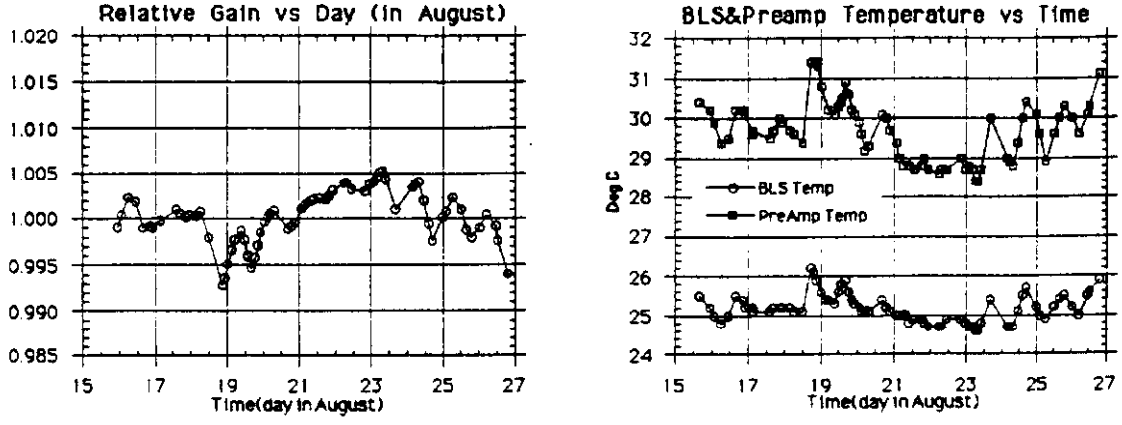

Figure 5: (a) Time dependence of the normalized gain value of a single calorimeter readout channel. (b) Time dependence of the BLS and preamp temperatures for the same time span.

Figure 5b shows the BLS and preamp temperatures as function of time for the same period. There is an obvious anti-correlation between the temperatures and the gains. Using the dependency between the gain and the temperatures of the BLS and preamp, a linear correction was applied to correct the gains for these temperature fluctuations, minimizing the rms of the gain distribution. The corrected gain distribution is shown in Figure 6. By applying the temperature correction the width of the gain distribution has been reduced by a factor of four to about 0.2%.

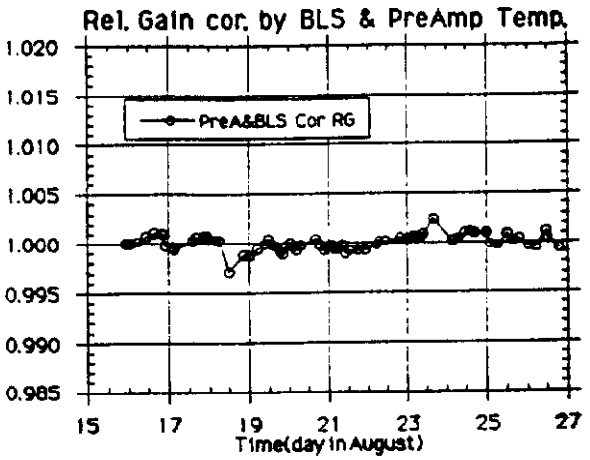

Figure 6: Normalized gain corrected for BLS and preamp temperature fluctuations.

5 Transfer of Calibration

Having established the absolute energy calibration of the calorimeter electronics in the controlled environment of a test beam, this calibration needs to be transferred to DØ. The full DØ experiment will have many more components and many parameters of the electronics system will be different. So, in order to use the calibration from the test beam a cross-calibration needs to be established between the test beam and DØ [6]. To this end a test station with its own pulser system was built.

In the calorimeter the energy of a shower initiated by a primary particle is calculated according to

$$E = \kappa \sum_i \frac{Q_i}{SF_i} \tag{3}$$

where the sum extends over all detector cells i along the path of the particle. Q_i is the charge deposited in calorimeter cell i and SF_i is the corresponding sampling fraction. The constant κ is determined by calibration. This equation can be rewritten in terms of the measured ADC voltages of the readout channels. The voltage V_i at the ADC is given by (see also equation 2)

$$V_i = R_i^{cal} \frac{Q_i}{C_F^i} \tag{4}$$

The same voltage V_i can be generated by injecting a charge Q_i' :

$$V_i = R_i^{pls} \frac{Q_i'}{C_F^i} \tag{5}$$

Here R_i^{cal} and R_i^{pls} are the response functions of readout channel i to calorimeter and pulser signals, respectively. These functions depend on many parameters of

the electronics circuit, in particular the FET transconductance, the detector capacitance, the β-value of the output transistor, the length of the cable from the preamp to the BLS and the timing of the peak signal. Using equations 4 and 5 equation 3 can be rewritten as

$$\begin{aligned} E &= \kappa \sum_i \frac{V_i \; C_F^i}{R_i^{cal} \; SF_i} \\ &= \kappa \sum_i \frac{R_i^{pls}}{R_i^{cal}} \; \frac{Q_i'}{SF_i} \end{aligned} \tag{6}$$

Whereas R_i^{pls} and R_i^{cal} individually depend on the parameters of the electronics circuit, the ratio is insensitive to these parameters and can be measured to an accuracy of better than 0.1%. In order to transfer the calibration to DØ a cross-calibration between the pulser system at DØ, with corresponding response function $R_i^{pls'}$, and the pulser system at the test beam needs to be established, as can be seen easily by writing equation 6 as

$$E = \kappa \sum_i \frac{R_i^{pls}}{R_i^{pls'}} \; \frac{R_i^{pls'}}{R_i^{cal}} \; \frac{Q_i'}{SF_i}$$

A complete set of pulser data has been taken with the test station during this calibration run to cross calibrate both pulser systems.

6 Conclusions

The DØ electronics was very reliable during the test beam run and performed as designed. The random and coherent noise per channel was 150-200μV and 5-7μV, respectively. Pedestals were stable to within 0.4%. After correcting for temperature fluctuations in the electronics a gain stability of better than 0.2% was reached. The linearity of the pulser system is better than 0.5% for all channels. To transfer the calibration to DØ a complete set of pulser data has been taken with a PC-based pulser test station.

7 Acknowledgements

I would like to thank my DØ colleagues for their help in preparing this report

References

1. A. Spadafora, "*Performance of the* DØ *Endcap Electromagnetic Calorimeter*", These proceedings.

2. N. Amos, "*The Performance of the* DØ *End Cap Hadronic Calorimeter Modules*", These proceedings.

3. R.D. Schamberger, "DØ *Calorimeter Electronics*", Proceedings of the Second International Conference on Advanced Technology and Particle Physics, Como, Italy, 11-15 June, 1990.

4. V. Radeka, S. Rescia, NIM **A265** (1988) 228.

5. P. Franzini, DØ-note 750, unpublished

6. J. Kourlas, J. Sculli, DØ-note 936, unpublished
   J. Kourlas, DØ-note 970, unpublished